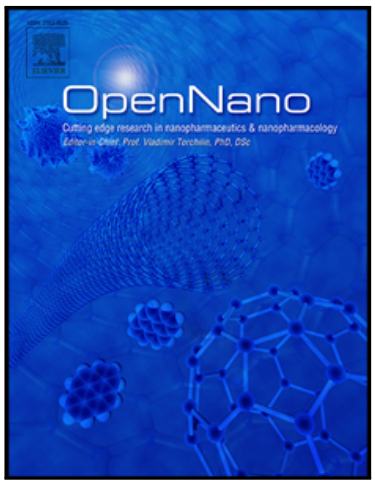

Green-synthesized silver nanoparticles using Aloe maculata extract as antibacterial agent for potential topical application

Gastón Franceschinis , Mariana Beverina , Merlina Corleto , Ayelen Morena Sosa , Cristian Lillo , Lucrecia Arias Casará , Silvia del Valle Alonso , Paulo Maffia , Jorge Montanari , Maria Eugenia Tuttolomondo , Maria Natalia Calienni

PII: S2352-9520(23)00027-0
DOI: https://doi.org/10.1016/j.onano.2023.100148
Reference: ONANO 100148

To appear in: *OpenNano*

Received date: 11 October 2022
Revised date: 6 April 2023
Accepted date: 9 April 2023

Please cite this article as: Gastón Franceschinis , Mariana Beverina , Merlina Corleto , Ayelen Morena Sosa , Cristian Lillo , Lucrecia Arias Casará , Silvia del Valle Alonso , Paulo Maffia , Jorge Montanari , Maria Eugenia Tuttolomondo , Maria Natalia Calienni , Green-synthesized silver nanoparticles using Aloe maculata extract as antibacterial agent for potential topical application, *OpenNano* (2023), doi: https://doi.org/10.1016/j.onano.2023.100148

Green-synthesized silver nanoparticles using *Aloe maculata* extract as antibacterial agent for potential topical application

Gastón Franceschinis[1,2,‡], Mariana Beverina[3,‡], Merlina Corleto[4,5], Ayelen Morena Sosa[1,2], Cristian Lillo[5,6,7], Lucrecia Arias Casará[3], Silvia del Valle Alonso[1,2], Paulo Maffia[4,5], Jorge Montanari[5,6], Maria Eugenia Tuttolomondo[3], Maria Natalia Calienni[1,2,6*]

1 Universidad Nacional de Quilmes, Departamento de Ciencia y Tecnología, Laboratorio de Bio-Nanotecnología, Bernal, C.P. 1876 Buenos Aires, Argentina.

2 Grupo de Biología Estructural y Biotecnología (GBEyB), IMBICE (CONICET CCT-La Plata), C.P. 1906 Buenos Aires, Argentina.

3 INQUINOA-CONICET, Instituto de Química Física, Facultad de Bioquímica, Química y Farmacia, Universidad Nacional de Tucumán, San Miguel de Tucumán, C.P. 4000 Tucumán, Argentina.

4 Universidad Nacional de Hurlingham, Laboratorio de Aplicaciones Biotecnológicas y Microbiología (LAByM), Villa Tesei, C.P. 1688 Buenos Aires, Argentina.

5 Consejo Nacional de Investigaciones Científicas y Técnicas (CONICET), C.P. 1425 Ciudad Autónoma de Buenos Aires, Argentina.

6 Universidad Nacional de Hurlingham, Laboratorio de Nanosistemas de Aplicación Biotecnológica (LANSAB), Villa Tesei, C.P. 1688 Buenos Aires, Argentina.

7 Universidad Nacional de La Plata (UNLP), Instituto de Investigaciones Fisicoquímicas Teóricas y Aplicadas (INIFTA), CONICET, La Plata 1900, Argentina

* Correspondence: natalia.calienni@unahur.edu.ar

‡ Authors contributed equally

Abstract: Nowadays, antibiotic resistance poses a threat to public health worldwide. For this reason, non-traditional antibacterial products, such as silver nanoparticles (AgNPs), offer an opportunity to address this issue. Although AgNPs have been proven to be effective antimicrobial agents, we studied the antibacterial and antibiofilm effects of two novel AgNPs (AgNP-Aloe-1 and AgNP-Aloe-2) obtained by green synthesis, their cytotoxicity on a cell line derived from human keratinocytes, and their skin penetration. These AgNPs were obtained here for the first time from an *Aloe maculata* aqueous extract as a reducing and capping agent of Ag(I), with varying the initial silver concentrations (5 and 9 mM of $AgNO_3$ for AgNP-Aloe-1 and AgNP-Aloe-2, respectively). For all the assessments, these were compared with AgNPs obtained from a traditional chemical method employing hydroxylamine hydrochloride as a reducing agent and $AgNO_3$ (AgNP-$NH_2OH{\cdot}HCl$). The AgNPs were characterized physicochemically by TEM, DLS, Zeta potential, UV-Vis, fluorescence, and Raman spectroscopy. Additionally, the concentration of silver forming AgNPs and the reaction yield

were determined. Both green-synthesized AgNPs showed an improvement in the inhibition of bacterial growth after 24 hours of incubation for *E. coli* and *S. aureus*. AgNP-Aloe-1 presented a MIC 4 times lower for both bacteria compared to AgNP-$NH_2OH{\cdot}HCl$, while AgNP-Aloe-2 presented a MIC 32 and 8 time lower for *E. coli* and *S. aureus*, respectively. Moreover, they produced a decrease in the biofilm biomass formation from *P. aeruginosa* at lower concentrations (6.25 µg/ml for AgNP-Aloe-1 and 1.56 µg/ml for AgNP-Aloe-2) than AgNP-$NH_2OH{\cdot}HCl$ which only showed a reduction of 30% at the maximum concentration tested. However, AgNP-Aloe-1 and AgNP-Aloe-2 were less efficient in eradicating pre-formed biofilm. Even though AgNP-Aloe-2 showed a lower reaction yield (31.7%) compared to AgNP-Aloe-1 (68.5%), they showed the best antibacterial activity. On the other hand, green-synthesized AgNPs were mainly retained in the *stratum corneum* of intact skin and reached lower concentrations in the viable epidermis than AgNP-$NH_2OH{\cdot}HCl$. Moreover, AgNP-Aloe-1 and AgNP-Aloe-2 did not show cytotoxic effects on human keratinocytes at the antibacterial concentrations. Their improved performance and lower skin penetration could be attributed to their physicochemical properties, such as size (10-25 nm), charge (around -10 mV), and shape (tendency towards a spherical shape), but mainly to the presence of phytocompounds from the extract that remained attached to the AgNPs, as observed by Raman spectroscopy and UV-Vis. For the reasons mentioned above, these novel AgNPs obtained by a more environmentally friendly method have the potential to be used as antibacterial agents, particularly for topical applications.

Keywords: Silver nanoparticles, antibacterial, antibiofilm, skin penetration, cytotoxicity

1 Introduction

The development of new antibiotics in recent years has been slow and insufficient to deal with the growing threat of microbial resistance, which is listed as a top-ten threat to public health by the World Health Organization [1]. On average, resistance to new antibiotics appears 2-3 years after their market release [2]. One of the main strategies against this problem is the search for non-traditional antibacterial products, including monoclonal antibodies, bacteriophages, and diverse nanomaterials. In particular, the antimicrobial properties of silver nanoparticles (AgNPs) have been well known for many years [3]. Classic synthesis methods involve the use of toxic reagents, high pressure, and energy [4], but there has been a shift towards more environmentally friendly ways to produce them, known as biogenic or green synthesis [5]. In these approaches, AgNPs can be produced by diverse organisms and microorganisms. Synthesis using plant extracts is especially attractive because of its low cost, lack of toxic chemicals, and the presence of a wide variety of metabolites capable of reducing the silver ions, stabilizing and capping the just-produced nanoparticles without adding further reagents [6, 7]. Thus, the main features of the obtained AgNPs (e.g. their concentration, composition, size, and shape) will depend on the plant species and synthesis conditions. Medicinal plants are usually sources of a rich variety of antioxidants and other molecules of interest [8]. The use of their extracts and silver salts to synthesize AgNPs is relatively easy and more sustainable than traditional physical and chemical methods [9], and the presence of some plant compounds on the surface of the obtained nanoparticles has been previously reported [10]. *Aloe vera* has been widely reported as the vegetable source for the production of AgNPs, with good biocompatibility and interesting antibacterial properties [11,12]. Due to the large number of phytochemicals and the complex nature of plant extracts, it is difficult to identify a specific compound that acts as the reducing and stabilizing agent in the synthesis of AgNPs. The role of several

phytochemicals such as polyphenols (flavonoids, phenolic acid, and terpenoids) has been proposed, but the actual mechanism behind the phytosynthesis of metal nanoparticles is still unknown [7].

Aloe maculata, also known as *Aloe saponaria* and *Aloe latifolia*, is another species from the same genus that has been reported to be therapeutically successful for many skin conditions, such as diabetic wounds, boils, infections, and acutely inflamed injuries [13,14,15]. Moreover, *Aloe maculata* has been reported to have other medicinal uses as an anti-inflammatory and antioxidant agent [14,16,17]. The records related to the use of the plant to treat dermatological ailments caused by infections describe the topical application of fresh leaves or sap [16,17]. Some articles also report the antibacterial activity of the *Aloe maculata* leaves [18] and leaf extract [19]. However, the antibacterial activity of most plant species remains to be verified to this day, as most of the articles refer to ethnobotanical studies. Although the composition of *Aloe maculata* largely depends on the substrate [20] and the environmental conditions of growth, it contains saponins, flavonoids, phenolic acids, anthraquinones, lectins, and polysaccharides [16,21,22]. Analysis of *Aloe maculata* gel after the elimination of aloin by FT-IR and Raman spectroscopy showed that it mainly contains polysaccharides and a low amount of phenolic compounds [23]. Among the non-cellulosic polysaccharides, pectines and acemannan were the main components observed. Despite all these properties mentioned above, there are no reports to date on the use of this plant in AgNPs synthesis.

In this study, AgNPs were produced using both a chemical and a green method by employing an aqueous extract of *Aloe maculata*, and then characterized by comparing their antibacterial, cytotoxic, and physicochemical properties. Additionally, their skin penetration profiles were studied on human skin samples to explore their potential use in topical treatments for bacterial infections.

2 Materials and methods

2.1 Materials

The reagents $AgNO_3$, K_2CrO_4, and hydroxylamine hydrochloride ($NH_2OH{\cdot}HCl$) were from Cicarelli (Details omitted for double-anonymized reviewing). Crystal violet, 3-amino-7-dimethylamino-2-methylphenazine hydrochloride (neutral red), dimethyl sulfoxide, ethanol, methanol, and acetone were purchased from BioPack (Details omitted for double-anonymized reviewing). The salt 3-[4,5-dimethylthiazol-2-yl]-3,5-diphenyltetrazolium bromide (MTT) and Mueller Hinton broth were obtained from Life Technologies™ (Thermo Fisher Scientific Inc., Details omitted for double-anonymized reviewing). RPMI 1640 medium, fetal bovine serum, glutamine, penicillin, and streptomycin were obtained from Gibco (Waltham, MA, USA). 1,1-diphenyl-2-picrylhydrazyl (DPPH) was purchased from Sigma-Aldrich. All other reagents used were of analytical grade.

2.2 Synthesis of AgNPs

For the production of green-synthesized AgNPs, $AgNO_3$ was used as a silver precursor at concentrations of 5 mM (AgNP-Aloe-1) and 9 mM (AgNP-Aloe-2). The reducing and capping agent used was an aqueous extract of *Aloe maculata*, where 10 ml of the extract was added to 90 ml of the $AgNO_3$ solution. The same concentration of the extract was used in both cases. The plants used were grown without any synthetic fertilizers, herbicides, or pesticides at ‘Details omitted for double-anonymized reviewing’ (Latitude XX and Longitude XX, height above sea level: 1100 meters) and harvested in March 2021. The plants were identified by

Dr. Jaime from the 'Details omitted for double-anonymized reviewing', and leaves from 3-year-old plants were collected. External leaves placed in the lower part of the plant were selected. The leaves were cut into small pieces and heated in distilled water (ratio 1:10, leaves:distilled water) at 80°C for 10 minutes. The resulting yellow liquid was then filtered. For conventional AgNPs synthesis (AgNP-$NH_2OH{\cdot}HCl$), 1.11 mM of $AgNO_3$ was used as a silver precursor, and hydroxylamine hydrochloride ($NH_2OH{\cdot}HCl$) was used as reducing agent [24, 25]. Briefly, 300 µl of a 1 M NaOH solution was added to 90 ml of 0.06 M $NH_2OH{\cdot}HCl$ solution, and then 10 ml of the $AgNO_3$ solution was added dropwise to the mixture under vigorous stirring. Finally, a brown silver colloid was obtained with a final pH of 5.5, and the silver suspension was aged for 24 h. Both methods were carried out at room temperature with constant stirring until a color change, indicating the formation of nanoparticles. All solutions were prepared in purified Milli-Q water. After synthesis, all AgNPs were stored in the dark at room temperature. They were purified from the synthesis medium using centricons (Amicon® Ultra-0.5 Centrifugal Filter Devices, Merck, Darmstadt, Germany) with a membrane of cellulose with a molecular cutoff of 3 kDa, and were kept in Milli-Q water. Two independent batches of AgNPs were obtained using extracts from different plants harvested at the same time and compared.

2.3 Determination of the AgNPs concentration

To determine the concentration of silver that formed AgNPs, the medium removed from the AgNPs purification was analyzed. This medium contained an excess of unreacted $AgNO_3$, which was quantified using a gravimetric method. The unreacted $AgNO_3$ can react with a saturated solution of K_2CrO_4 to form Ag_2CrO_4 according to the following reaction:

$$AgNO_3 + K_2CrO_4 \rightarrow Ag_2CrO_4 \downarrow + 2KNO_3$$

The Ag_2CrO_4 forms a visible red precipitate in the reaction tube. It was filtered using a Whatman® N°41 filter and quantified on an analytical balance. Then, based on the exact initial amount of $AgNO_3$ used, the amount of silver that formed AgNPs was calculated.

2.4 Physicochemical characterization

To confirm the formation of AgNPs and their characteristic surface plasmon resonance, a spectral scan ranging 300 to 600 nm was performed (Jasco V-550 spectrophotometer, Japan). Additionally, the fluorescence emission of the AgNPs was studied (FluoroMate FS2, SCINCO, South Korea).

The size and shape of the AgNPs just after synthesis were assessed by transmission electron microscopy (TEM) using a Zeiss Libra 120 microscope (Carl Zeiss AG, Oberkochen, Germany). Changes in the size and stability of the AgNPs over time were monitored using Dynamic Light Scattering (DLS) and Zeta Potential (Zetasizer Nano, Malvern Instruments, UK). The measurements were carried out in triplicate after six months of synthesis at 25 ± 0.1°C.

The retention of some components of the extract in the AgNPs obtained by green synthesis was assessed using Raman spectroscopy. Raman spectra were measured in the 3500–100 cm^{-1} region employing a Thermo Scientific DXR Raman microscope (Waltham, MA, USA), with a resolution of 5 cm^{-1}. A diode-pumped solid-state laser of 532 nm was employed as an excitation source. The spectra were analyzed using the OMNIC™ program for dispersive Raman.

The Folin-Ciocalteu reactive technique adapted to lower volumes [26] was used in triplicate to determine the total polyphenolic compounds present in both the extract and the remains on the AgNPs. Gallic acid was used as a reference. Aliquots containing 100 µl of each sample were combined with 650 µl of water and 125 µl of Folin-Ciocalteu reactive under continuous and vigorous agitation. After 3 minutes, 125 µl of Na_2CO_3 (2%) was added, and the samples were incubated for 2 hours while being shaken every 15 minutes. A calibration curve was created using gallic acid in the concentration range of 0 to 5 mg/ml. Absorbance was measured at 760 nm.

To assess the antioxidant behavior of the formulations, the free radical scavenging activity was measured in triplicate using the DPPH colorimetric method [26]. Briefly, 20 µl of the sample was added to 980 µl of a 0.003% (w/v) solution of the stable free radical DPPH in methanol. The samples were incubated for 30 min in darkness at room temperature, and then the remaining reactive was quantified by measuring its absorbance at 515 nm. The absorbance of the DPPH solution was used as the inhibition blank. Butylated hydroxytoluene (BHT) was used as the positive control for antioxidant activity. The inhibition percentage (I%) was calculated using the following equation:

$$I\ (\%) = [(Abs_{blank} - Abs_{sample}) / Abs_{blank}] \times 100$$

2.5 Cytotoxic effects on human keratinocytes

In vitro studies were conducted using the HaCaT cell line, which is derived from immortalized human skin keratinocytes. The cell line was obtained from the cell bank of the 'Details omitted for double-anonymized reviewing'. The cells were cultured in RPMI 1640 medium supplemented with 2 mM glutamine, 100 IU/mL penicillin, 100 µg/mL streptomycin, 0.25 µg/mL of amphotericin B, and 10% heat-inactivated fetal bovine serum (FBS) at 37°C with 5% CO_2.

To assess cell viability after 24 hours of incubation with AgNP-Aloe-1, AgNP-Aloe-2, and AgNP-$NH_2OH{\cdot}HCl$, the MTT, crystal violet (CV), and neutral red (NR) assays were performed in triplicate, following the protocols reported in Calienni et al. (2021) [27]. A total of $1x10^4$ cells/well were seeded on 96-well flat-bottom microplates. After 24 hours, the culture medium was replaced with 90 µl of fresh medium without FBS to avoid the protein corona effect, and 10 µl of AgNP dilution was added. The concentration of silver forming AgNPs tested ranged from 100 to 1600 µg/ml. After incubation, the medium was removed, the cells were washed three times with phosphate-buffered saline pH 7.4 (PBS), and the MTT, CV, and NR assays were performed.

The absorbance measurements were performed using the multi-mode reader Cytation 5 (BioTek Instruments, USA). The percentage of cell viability was calculated according to the following equation, where "Abs-T" is the absorbance of treated cells and "Abs-C" is the absorbance of the untreated control.

$$\text{Cell viability}\ (\%) = (Abs\text{-}T) / (Abs\text{-}C) \times 100$$

2.6 Antibacterial and antibiofilm properties of AgNPs

2.6.1 Bacterial strains and growth conditions

The representative Gram-negative strain *Escherichia coli* ATCC25922 and Gram-positive strain *Staphylococcus aureus* ATCC25923 were used to determine the minimal inhibitory concentration (MIC) of AgNPs. *Pseudomonas aeruginosa* M13513 [28] was used for biofilm test and it was selected for its ability to form biofilm *in vitro* on diverse surfaces. All strains

were grown in Mueller Hinton broth at 37°C, and assays were carried out in flat-bottom 96-well microplates seeding $5x10^5$ CFU/100 µl in each well.

2.6.2 Determination of the MIC

The MIC was determined using the standard Broth Microdilution Method as recommended by the Clinical and Laboratory Standards Institute (CLSI) [29]. Triplicate tests were carried out for each AgNP and for the *Aloe maculata* extract against *E. coli* and *S. aureus* to determine the MIC. The MIC was also determined for *P. aeruginosa* for subsequent biofilm studies. Concentrations of each AgNP starting from 800 µg/ml were tested, and serial dilutions were made until the MIC was obtained. Growth control wells with untreated cells and wells with cell-free culture medium as a control for contamination were included in the microplates. The microplates were incubated for 24 hours at 37°C, and OD was measured at 600 nm using a microplate reader (RT2100, Rayto Life and Analytical Sciences Co., Ltd, China).

2.6.3 Inhibition of biofilm formation

The study on *P. aeruginosa* biofilm formation inhibition was conducted by incubating the bacteria with AgNPs at sub-MIC values in Mueller Hinton broth for 24 hours at 37°C [30]. The maximum concentration tested was 0.5 × MIC, and non-incubated bacteria and free-cell medium were included in the study. The assay was carried out in sextuplicate. After incubation, the OD at 595 nm was measured to assess bacterial growth. Each well was washed twice with PBS, taking care not to detach the biofilm formed, removing non-adherent cells. The biofilm formed was incubated with 100 µl of methanol for 10 minutes and with 100 µl of CV solution (1% v/v) for 5 minutes. The dye was removed, wells were washed twice with distilled water, and the microplate was allowed to dry at 37°C for 30 minutes. Finally, 100 µl of acetic acid solution (33% v/v) was added, and after 15 minutes of incubation, the samples were homogenized, and the OD at 595 nm was measured in a microplate reader to quantify the biofilm formation inhibition.

2.6.4 Eradication of pre-formed biofilm

To determine the ability of AgNPs to destroy pre-formed *P. aeruginosa* biofilms, concentrations of each nanoparticle starting from 5 times the MIC value were tested, with maximum concentrations up to 32 times the MIC. Sextuplicate determinations were performed after making serial dilutions in Mueller Hinton broth. *P. aeruginosa* was allowed to form a biofilm in microplates for 24 hours at 37°C. The supernatant was carefully removed and 100 µl/well of AgNPs dilutions were added along with non-incubated biofilms and free-cell medium. The microplate was incubated for 24 hours at 37°C. The supernatant was removed and each well was washed thrice with PBS. Then, 100 µl of MTT solution (0.05 mg/ml in PBS) were added to each well and bacteria were incubated for 3 h at 37°C. The samples were homogenized and the OD at 595 nm was measured in a microplate reader to quantify the effectiveness of AgNPs in killing bacteria in pre-formed biofilms.

2.7 Skin penetration assays

2.7.1 Skin incubation and tape stripping

The Saarbrücken Penetration Model (SPM) [31] was used to evaluate the *ex vivo* skin penetration of AgNPs. Skin samples were obtained from a healthy 44-year-old Caucasian female donor who underwent an abdominoplasty. The subcutaneous tissue was removed,

and the skin surface was cleaned with PBS. The skin explants were wrapped in aluminum foil and stored in hermetic polyethylene bags at −20 °C until use for a maximum period of six months. Skin disks of 4.9 cm^2 were punched out from explants and placed in SPM Teflon devices with the *stratum corneum* (SC) facing up [32]. A filter paper embedded with PBS was added to the bottom of the devices to simulate the transdermal humidity gradient present in the skin. The explants consisted of the SC, viable epidermis, and dermis. Each skin disk was incubated with 50 µl of the different AgNPs (1600 µg/ml), which were applied to the skin surface as 2.5 µl drops. The skin disks were then incubated under non-occlusive conditions at 35 ± 1 °C for 1 h. After the incubation, the skin disks were mounted on an expanded polystyrene foam block and successively stripped with 20 pieces of adhesive tape (Details omitted for double-anonymized reviewing) to remove the SC, covering the whole surface of the skin. A 2-kg weight was applied over each tape for 10 seconds. The tapes were grouped according to shallow SC (tapes 1–10) and deep SC (tapes 11–20). The remaining skin below the SC, which consisted of the viable epidermis and the dermis (VED), was cut into small pieces and homogenized. Skin samples that were not incubated with AgNPs but were treated identically to the others were included as controls. These assays were performed in triplicate.

2.7.2 AgNPs detection in the skin layers

The tapes and VED were treated with 1 ml of 1 M HNO_3 solution to extract silver from AgNPs present in the samples. Each sample was vigorously shaken for 2 minutes and allowed to incubate for 1 hour. After this, the acid was neutralized, and the samples were brought to a pH between 7.5 and 8.0 using a 2 M NaOH solution. The solid content of the samples was removed, and 1 ml of 25 % w/v K_2CrO_4 solution was added, and the mixture was allowed to incubate for 1 h protected from light. From each sample, 1 ml was centrifuged at 14,000 rpm for 20 minutes, and three aliquots of each one were seeded in a 96-well microplate to measure absorbance at 375 nm using Cytation 5. The data were normalized to the total amount of AgNPs recovered from the skin explants.

2.7.3 Ethics Statement

Protocols involving human skin samples were approved by the Ethics Committee of the 'Details omitted for double-anonymized reviewing'.

2.8 Statistical analysis

The data were analyzed using one-way ANOVA and Dunnett's multiple comparison tests. Each treatment was compared to the control. When it was necessary to compare only two variables, the data were analyzed using Student's t-test. GraphPad Prism 6.0 (GraphPad Software Inc., San Diego, CA, USA) was used for all statistical analyses. Only values with $p < 0.05$ were considered statistically significant.

3. Results and discussion

3.1 AgNPs concentration

Table 1 displays the concentration values and reaction yields for each AgNP. Both AgNPs obtained from green synthesis showed similar concentrations of silver forming nanoparticles regardless of the initial concentration of $AgNO_3$. AgNP-Aloe-1 exhibited a reaction yield of around 69%, while AgNP-Aloe-2 presented a yield of approximately 32%. On the other hand,

AgNP-$NH_2OH{\cdot}HCl$ showed a yield of 87%. Good reproducibility between batches was observed in all cases.

Table 1. Concentration values of silver forming AgNPs measured in two independent batches, their averages, average reaction yield, and corresponding standard deviation (SD).

Nanoparticle	1st batch concentration (mM)	2nd batch concentration (mM)	Average concentration (mM)	Reaction yield (%)
AgNP-Aloe-1	3.05 ± 0.21	3.80 ± 0.14	3.42 ± 0.50	68.5 ± 10.6
AgNP-Aloe-2	2.65 ± 0.35	3.05 ± 0.07	2.80 ± 0.30	31.7 ± 3.1
AgNP-$NH_2OH{\cdot}HCl$	1.01 ± 0.01	0.91 ± 0.01	0.96 ± 0.07	86.5 ± 6.4

3.2 Physicochemical characterization

3.2.1 Spectroscopic analysis

The absorption spectra of AgNP-Aloe-1 and AgNP-Aloe-2 did not exhibit a single absorption band (Fig. 1A) as expected for green-synthesized nanoparticles [33]. For AgNP-$NH_2OH{\cdot}HCl$ it was only possible to observe the characteristic absorption band close to 420 nm (λ = 422 nm) (Fig. 1B), which is attributed to the surface plasmon resonance of AgNPs [34]. After deconvolving the absorbance spectra of AgNP-Aloe-1 and AgNP-Aloe-2 using the OriginPro 2019b software, three possible absorption bands were observed (Fig. 1C and D). For both AgNPs, a band around 390 nm can be assigned to the plasmon resonance. The other two bands at higher wavelengths (around 470 nm and above 500 nm) could be associated with the components of the extract that are part of the AgNPs, but also could be related to the presence of aggregates in the suspension [35]. These aggregates would not be an unlikely event in the recently synthesized AgNP-Aloe-1 and AgNP-Aloe-2 since they were not stabilized with any additional chemical agent. Only the *Aloe* extract and $AgNO_3$ were utilized for their synthesis.

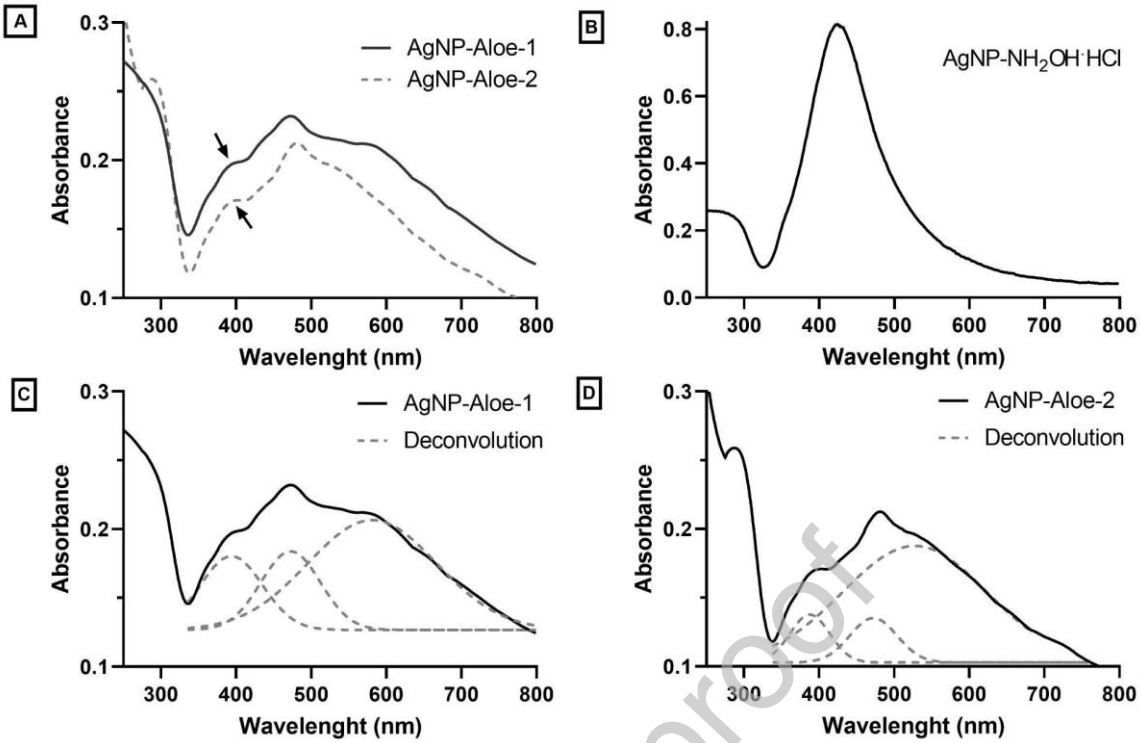

Figure 1. Absorbance spectra of AgNP-Aloe-1 and AgNP-Aloe-2 (A) and AgNP-NH_2OH·HCl (B) of the first batch. Arrows indicate a possible band around 390 nm for both green synthesized nanoparticles that can correspond to the surface plasmon resonance. Spectra and their deconvolution into three possible absorption maxima for AgNP-Aloe-1 –around 390, 470 nm, and 580 nm– (C) and AgNP-Aloe-2 –around 390, 470 nm, and 530 nm– (D) are also shown.

On the other hand, the AgNPs exhibited moderate fluorescence emission with different emission maxima when they were excited with λ = 390 nm (Fig. 2). The AgNP-Aloe-2 showed the lowest fluorescence emission intensity with a maximum at 555 nm, while the AgNP-Aloe-1 showed the highest fluorescence intensity with a peak at 570 nm (about 55% more intensity than AgNP-Aloe-2). AgNP-NH_2OH·HCl exhibited an emission maximum of around 540 nm with an intermediate intensity between both green-synthetized AgNPs.

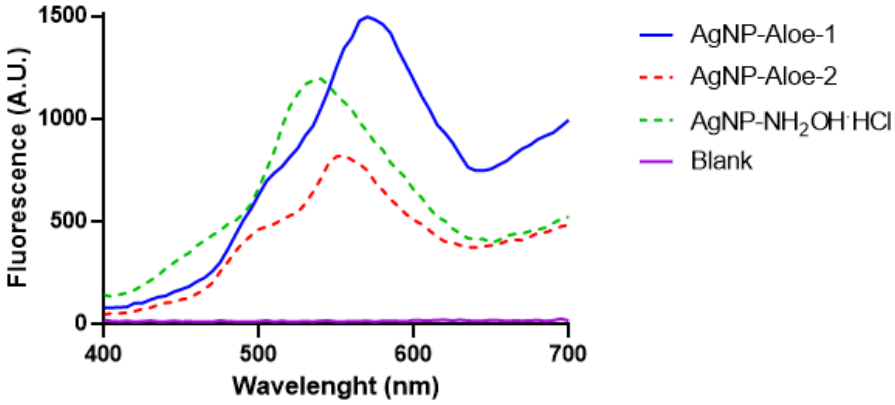

Figure 2. Fluorescence emission spectra (λexc = 390 nm) for the AgNPs of the first batch and a blank of ultrapure water.

Raman spectroscopy was used to confirm the presence of different organic functional groups from the *Aloe maculata* extract, which were retained in the AgNPs, and to compare their behavior (Fig. 3). Both AgNPs exhibited a shoulder at 1649 cm^{-1} and a broad band at 1602 cm^{-1} corresponding to C=O groups. However, in the extract spectrum, these bands were observed at 1745 and 1730 cm^{-1}, respectively. This shift could be attributed to the interaction of the AgNPs with the carbonyl groups of the polysaccharides mainly present in the *Aloe* extract [23]. The band at 1335 cm^{-1} is attributed to -CH_3 deformations, while the bands at 1350-1410 cm^{-1} correspond to the asymmetric bending of -CH_3 groups and -C-OH bending in experimental Raman. This first band was further intensified for AgNP-Aloe-1, possibly due to the interaction of the CH group with the nanoparticles.

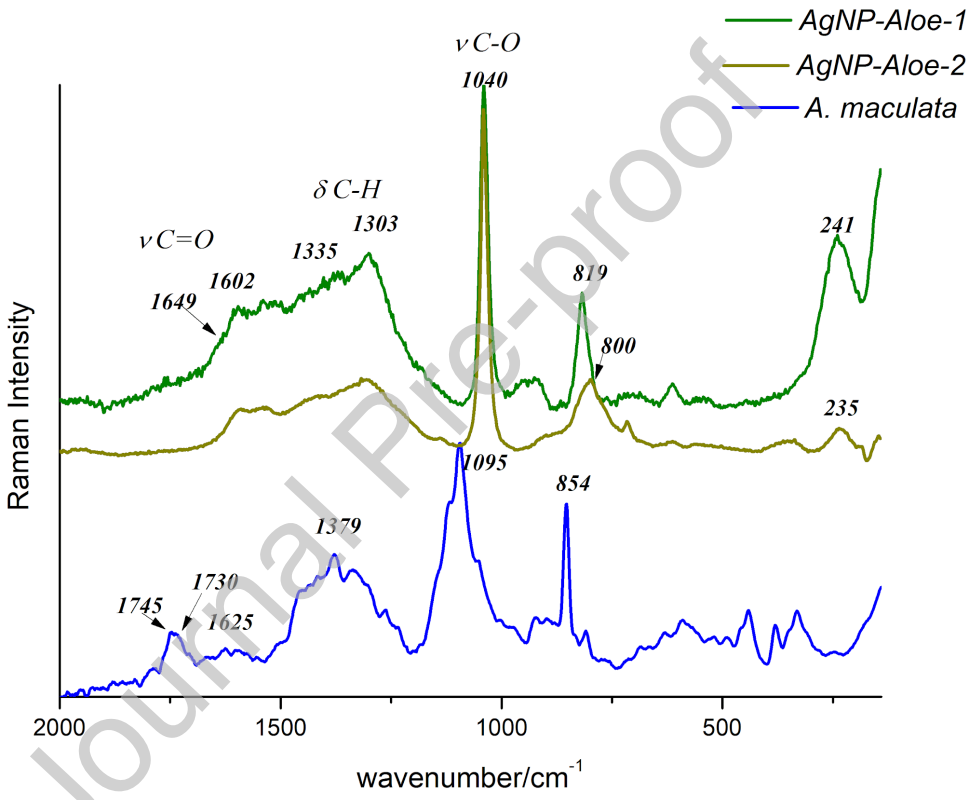

Figure 3. Raman spectra of the dried extract from *Aloe maculata*, AgNP-Aloe-1, and AgNP-Aloe-2, λexc = 532 nm. Spectra are shown offset for easier visualization.

According to Beverina et al. (2022), the theoretical Raman spectrum of the dried extract from *Aloe maculata* displays a series of bands observed in the 1100-1000 cm^{-1} region, which can be attributed to the C-C and C-O stretching vibrations. The position and intensities of these bands are determined by the different positions of the corresponding C-O bonds existing in the acemannan chain. This group of bands is usually the most intense one in the Raman spectra. These bands appeared for the extract as a broad and intense band centered at 1095 cm^{-1}, where some shoulders can be observed at 1116 and 1050 cm^{-1}. In the spectra that correspond to AgNP-Aloe-1 and AgNP-Aloe-2, the band present at 1095 cm^{-1} for the extract appeared much more intense at 1040 cm^{-1} for both nanoparticles. This shift may be due to the electrostatic interaction between the surface silver and the C-O groups of the

polysaccharides. On the other hand, a prominent and narrow band can be seen at 854 cm^{-1} in the spectrum of *Aloe maculata* extract. This band also appears approximately at the same position in the theoretical Raman spectrum and can be attributed to the C-O stretching vibration of the CH_3-C(O)-O group in the ester group, as well as the –C(O)-O- corresponding to the anomeric one. In the AgNPs spectra, it appeared at 819 cm^{-1} (AgNP-Aloe-1) and 800 (AgNP-Aloe-1) cm^{-1}. This behavior can be due to the strong interaction of this group with the plasmon of the nanoparticles and was stronger for the AgNP-Aloe-2. Moreover, the band corresponding to the stretching Ag--O=C- mode appeared at 241 cm^{-1} for the AgNP-Aloe-1 and at 235 cm^{-1} for the AgNP-Aloe-2. These bands did not appear in the spectrum of *Aloe*, as expected, because they correspond to the interaction of the C=O group of the acemannan with the reduced silver of AgNPs. In the spectrum of the *Aloe* extract, bands at 1625, 635, and 600 cm^{-1} associated with the ester groups can also be observed, which appeared only in the AgNP-Aloe-1 spectrum. Furthermore, the intensity of the Ag--O band at 241 cm^{-1} of the AgNP-Aloe-1 was three times higher than the same band of the AgNP-Aloe-2 at 235 cm^{-1}. This could be related to a higher interaction between the surface plasmon of AgNP-Aloe-1 and the ester groups of the extract in comparison with AgNP-Aloe-2.

Several studies have been performed to elucidate the mechanism involved in the synthesis of metallic nanoparticles, including AgNPs, using plant extracts. However, the mechanisms behind the phytosynthesis of nanoparticles are still unknown. The most accepted mechanism mainly involves the presence of reducing and stabilizing agents in the plant extract. Some of the phytocompounds proposed to have a role in the synthesis are polyphenols (flavonoids, phenolic acid, and terpenoids), organic acids, and proteins [7]. Some of these are thought to play a dual role as both reducing and stabilizing agents. Nevertheless, the complex nature of the extract and the large number of phytochemicals that are present make it difficult to identify the individual role of each specific component in the synthesis process. Figure 4 presents a schematic representation of the formation process.

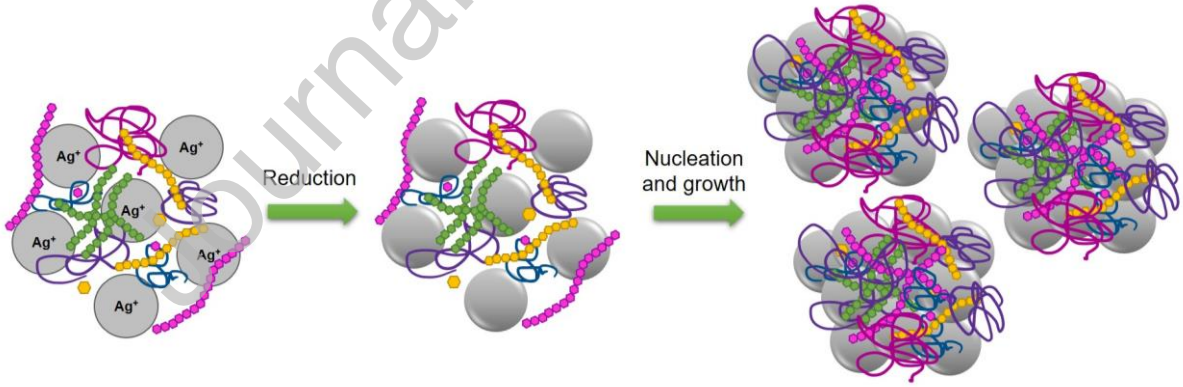

Figure 4. Schematic representation of the synthesis process for the AgNP-Aloe-1 and AgNP-Aloe-2 starting from an aqueous solution of $AgNO_3$ and an aqueous extract of *Aloe maculata* leaves.

3.2.2 Size, shape, and colloidal stability

Based on the TEM micrographs (Fig. 5) obtained from the newly synthetized AgNPs, it was observed that AgNP-Aloe-1 and AgNP-Aloe-2 were amorphous but tended towards a spherical shape. In the case of AgNP-$NH_2OH{\cdot}HCl$, they also had a quite spherical shape. The AgNPs presented a size distribution between 10 to 25 nm.

Moosa et al. (2015) obtained AgNPs with an *Aloe vera* extract using a similar method of extraction and synthesis of AgNPs [36]. From AFM images, they determined that the AgNPs had an average size of 35.26 nm when 5 mM of $AgNO_3$ was used as the precursor and 55.38 nm for 9 mM of $AgNO_3$. The differences in size compared to the AgNPs obtained here from *Aloe maculata* could be related to differences in the composition and concentracion of relevant phytochemicals in both extracts, and therefore, in the conformation of the final AgNPs. These differences may affect the reducing capacity, with consequence in the amount of reducted silver that can nucleate and form the nanoparticles, as well as their capping. The capping determines the size of the AgNPs as well as their tendency to agglomerate. However, it is important to mention that there are variations between the measurements of the mean size carried out with different methodologies. Therefore, a direct comparison between both studies cannot completely be done.

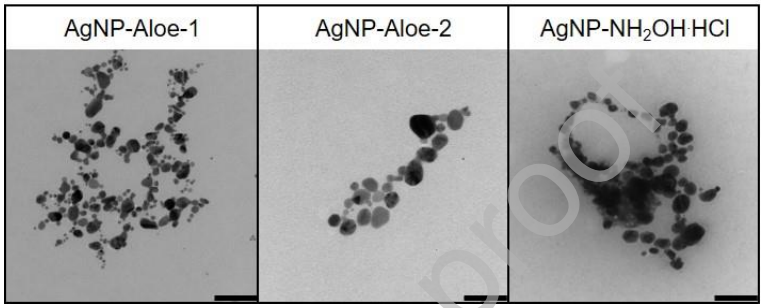

Figure 5. TEM micrographs of AgNP-Aloe-1 (50.000x), AgNP-Aloe-2 (100.000x), and AgNP-$NH_2OH{\cdot}HCl$ (50.000x), all from the first batch. The scale bar for the 50,000x micrographs corresponds to 100 nm, and for the 100,000x micrograph, it corresponds to 50 nm.

Six months after the synthesis, the size of the AgNPs was measured in triplicate by DLS for both batches to study their stability over time. It was observed that there was a tendency for all three AgNPs to aggregate over time, resulting in a polydisperse size distribution when observed as intensity plots, but this effect was more pronounced for the AgNPs synthesized through green synthesis. When the size distribution was observed for each case as the percentage of number, it was monodisperse. The average size of AgNP-$NH_2OH{\cdot}HCl$ (around 12 nm) was similar to that determined by the TEM micrographs obtained just after the synthesis, whereas both AgNP-Aloe-1 and AgNP-Aloe-2 presented higher average sizes (more than 90 nm) six months after the synthesis (Table 2). The size variation between batches was significant for AgNPs synthesized through green synthesis, whereas AgNP-$NH_2OH{\cdot}HCl$ showed practically the same average size (Fig. 6A). On the other hand, the high polydispersity index (PDI) values (Fig. 6B, Table 2) for both batches of all AgNPs corresponded with the polydispersity observed in most of the histograms obtained by DLS (when observed as the percentage of intensity). This polydispersity is possibly associated mainly with the formation of aggregates of different average sizes but also with the shape of the AgNPs, which are not perfect spheres –one of the assumptions of the DLS analysis. Likewise, as mentioned before, it was observed in all cases that most of the AgNPs were around an average size in each suspension and that larger sizes represented a considerably smaller population of the set of nanoparticles formed.

Table 2. Hydrodynamic size and PDI measured by DLS and Zeta potential of AgNPs six months after the synthesis. The data are shown as mean ± SD (n = 3). The average size

reported was determined based on the number size distribution graphs, which show the size range of most of the AgNPs present in the suspension.

		AgNP-Aloe-1	AgNP-Aloe-2	AgNP-NH_2OH·HCl
Size (nm)	**First batch**	94.01 ± 7.76	195.12 ± 8.69	11.86 ± 2.17
	Second batch	231.80 ± 20.09	117.22 ± 42.57	11.93 ± 2.78
PDI	**First batch**	0.359 ± 0.026	0.412 ± 0.062	0.449 ± 0.025
	Second batch	0.327 ± 0.020	0.420 ± 0.049	0.487 ± 0.019
Zeta potential (mV)	**First batch**	-9.96 ± 0.77	-9.73 ± 0.68	-18.15 ± 0.50
	Second batch	-24.83 ± 0.75	-4.83 ± 0.49	-15.17 ± 1.95

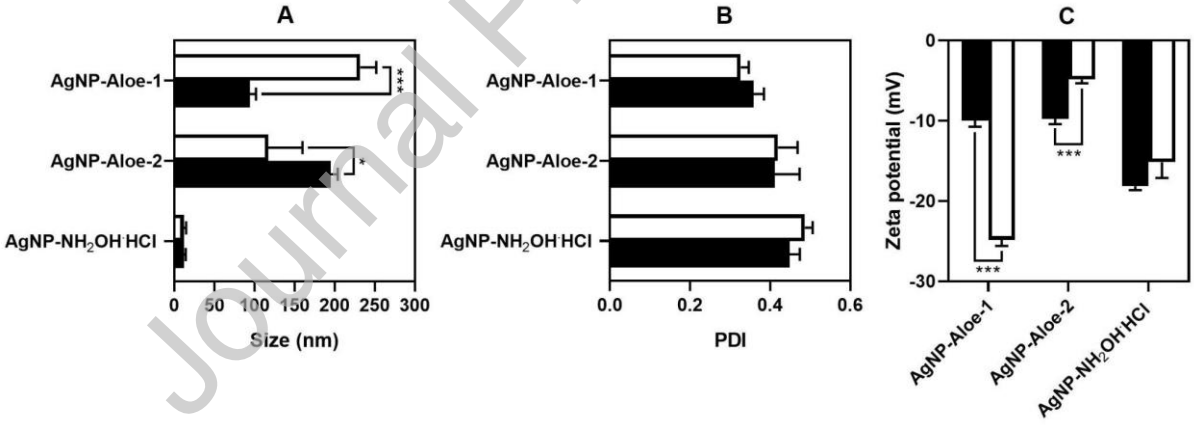

Figure 6. Average size (A), PDI (B), and Zeta potential (C) of AgNP-Aloe-1, AgNP-Aloe-2, and AgNP-NH_2OH·HCl from the first (black bars) and second (white bars) batch obtained six months after the synthesis. Average size reported was determined based on the number size distribution graphs, which show the size range of most of the AgNPs present in the suspension. The data are shown as mean ± SD (n = 3). Statistical analysis was performed using the Student's t-test to compare between batches, * $p < 0.05$, *** $p < 0.0005$.

The AgNPs synthesized through green synthesis exhibited a slightly negative surface charge, with the exception of the second batch of AgNP-Aloe-1, which had a charge of -24.83 mV (Fig. 6C, Table 2). Likewise, for the same nanoparticles in the first batch, the potential was also less than -10 mV. Although extracts from plants harvested at the same time were used, variations in composition between batches may lead to AgNPs with different

surface features. The low Zeta potentials partly explain the tendency of AgNPs to aggregate over time, as observed by DLS, due to low electrostatic repulsion. AgNP-$NH_2OH{\cdot}HCl$ presented the farthest Zeta potential values from zero, indicating that they would be more colloidally stable over time.

The amount of polyphenolic compounds in each sample was expressed in milligrams of gallic acid equivalents per ml. While the pure extract contained 1.28 ± 0.48 mg of gallic acid equivalents per ml, this value dropped to zero for both green-synthesized AgNPs. On the other hand, the I% that corresponds to the amount of radical DPPH scavenged did not show significant differences between the pure extract and the green-synthesized nanoparticles in their original synthesis medium (Table 3). Remarkably, the percentage increased slowly after purification, which was also observed in the synthesis of AgNPs from other plant extract [37]. Thus, both AgNPs did not contain polyphenolic compounds, consistent with the Raman spectroscopy analyses that did not detect signals of polyphenolic compounds for AgNPs. Therefore, the antioxidant activity is not due to polyphenols, but it is possible that it is related to polysaccharides. *Aloe maculata* has a high content of polysaccharides [23], which were retained in the AgNPs as determined by Raman spectroscopy (Fig. 3). The *in vitro* antioxidant activity of *Aloe maculata* was previously reported in the literature [38], and it was also corroborated that polysaccharides have antioxidant activity [39].

Table 3. Antioxidant activity determined as the percentage of inhibition that corresponds to the amount of radical DPPH scavenged. The data are shown as mean ± SD (n = 3) and were analyzed using one-way ANOVA and the multiple comparisons tests of Dunnett. Each AgNP was compared to the plant extract, **** $p < 0.0001$. Only significant differences were observed between the purified AgNPs and the pure extract.

	***Aloe maculata* extract**	**AgNP-Aloe-1** (with synthesis medium)	**AgNP-Aloe-2** (with synthesis medium)	**AgNP-Aloe-1** (without synthesis medium)	**AgNP-Aloe-1** (without synthesis medium)
Antioxidant activity (% of inhibition)	51.03 ± 1.57	51.22 ± 1.09	51.00 ± 1.28	66.25 ± 0.58****	70.76 ± 3.47****

The physicochemical features of AgNPs vary significantly depending on the precursors used as can be observed in bibliography. This is due to the close relationship between the final characteristics of the nanoparticles and the synthesis process, as well as the amount and nature of the precursor. In green synthesis, the reproducibility is challenging because of the complexity of the biological resource used and its inherent variations. Although AgNP-Aloe-1 and AgNP-Aloe-2 presented had similar sizes immediately after synthesis for both batches, their tendency to aggregate in aqueous suspension differed after six months, as observed by DLS. This may be related to the phytochemicals retained in each batch of the AgNPs. As mentioned before, the actual mechanism of green synthesis using plant extract is still unclear [7], and it is necessary to continue characterizing the aqueous extract obtained from *Aloe maculata* to improve the reproducibility of further AgNPs batches. Additionally, it is

important to study possible methods of preserving these AgNPs over time, such as lyophilization.

3.3 Cytotoxic effects on human keratinocytes

The cytotoxicity of the three AgNPs studied in HaCaT cells was determined using the MTT, CV, and NR assays after 24 hours of treatment (Fig. 7). The MTT test did not show a reduction in cell viability below 75% for any of the treatments, indicating that mitochondrial activity was not significantly altered. Although all concentrations studied showed statistically significant differences compared to the untreated control, the results were not biologically relevant. Only AgNP-Aloe-1 showed a concentration-dependent tendency to decrease viability, which was not evident with the other two AgNPs. With the CV test, statistically significant differences with the untreated control were observed for several conditions tested. However, the reduction in viability percentage was not significant from a biological standpoint since viability did not drop below 80% in any of the studied conditions.In contrast, the NR assay showed a concentration-dependent cytotoxic effect from both AgNPs synthesized using the green method in the range studied. This indicates that both AgNPs were likely affecting the ability of the cells to maintain pH gradients [40] or the integrity of the cell membranes, leading to decreased retention of the NR. This effect on cell membranes is typical of AgNPs [41].

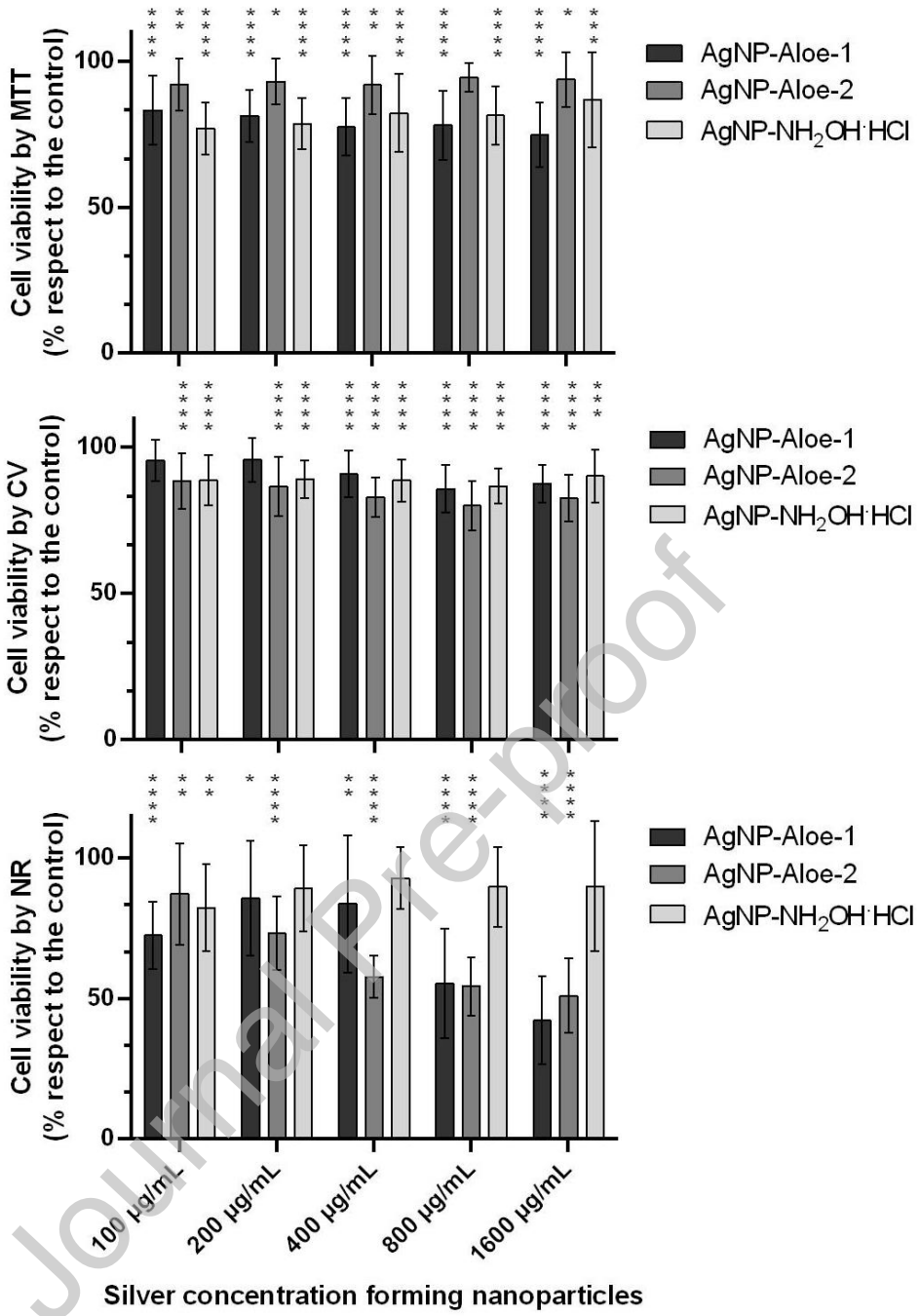

Figure 7. Percentage of cell viability of HaCaT line determined by MTT, CV, and NR assays after 24 hours of incubation with different concentrations of AgNPs. The data are shown as mean ± SD (n = 3) and were analyzed using one-way ANOVA and the multiple comparisons tests of Dunnett. Each treatment was compared to the untreated control, * $p < 0.05$, ** $p < 0.004$, *** $p < 0.0006$, **** $p < 0.0001$. Even though there were statistically significant differences with respect to the control in MTT and CV assays, the results were not biologically relevant because the treatments did not significantly reduce cell viability. Only the NR assay showed a viability reduction higher than 20%.

3.4 Antibacterial and antibiofilm properties of AgNPs

In vitro tests were conducted to verify the efficacy of different nanoparticles against microbial agents. The antibacterial activity of AgNPs was studied by determining the MIC, the inhibition of biofilm formation, and the ability to eradicate pre-formed biofilms.

The results showed inhibition of bacterial growth by AgNPs. Green-synthesized AgNPs were more effective than AgNP-$NH_2OH{\cdot}HCl$, as they generated growth inhibition at lower concentrations in both Gram-negative and Gram-positive bacteria (Table 4). Besides, AgNP-Aloe-2 was more toxic to both strains than AgNP-Aloe-1. Evaluation of the antimicrobial activity of AgNPs demonstrated different rates of inhibition depending on the strain. *E. coli* was more susceptible to all three AgNPs than *S. aureus*. This difference could be related to the variation in the composition and structure of the cell wall between Gram-negative and Gram-positive bacteria. Other studies have reported that several AgNPs tend to accumulate in the outer membrane of *E. coli*, resulting in increased permeability and cell death [42]. Conversely, the *Aloe maculata* extract did not exhibit antimicrobial activity against *E. coli*, *S. aureus*, and *P. aeruginosa*.

Table 4. MIC values for AgNPs determined in *E. coli*, *S. aureus*, and *P. aeruginosa*.

AgNPs	***E. coli***	***S. aureus***	***P. aeruginosa***
AgNP-Aloe-1	100 µg/mL	200 µg/mL	25 µg/mL
AgNP-Aloe-2	12.5 µg/mL	100 µg/mL	25 µg/mL
AgNP-$NH_2OH{\cdot}HCl$	400 µg/mL	800 µg/mL	12.5 µg/mL

To analyze the capability of the AgNPs to inhibit *P. aeruginosa* biofilm formation, CV staining was performed after 24-hours incubation with sub-inhibitory concentrations (Fig. 8). The data showed that biofilm biomass decreased in a concentration-dependent manner in the presence of AgNP-Aloe-1 and AgNP-Aloe-2, with the minimum concentrations that can prevent the formation of biofilm being 0.25 × MIC and 0.0625 × MIC, respectively. On the other hand, AgNP-$NH_2OH{\cdot}HCl$ presented a small reduction of the total biomass at the highest concentrations (around 20% at 0.25 × MIC and 30% at 0.5 × MIC).

In order to study the effect of the AgNPs on the viability of bacteria conforming the pre-formed biofilm and exposed 24 hours to different supra-MIC values, the MTT test was performed. All AgNPs decreased cell viability (Fig. 8). In this case, AgNP-$NH_2OH{\cdot}HCl$ produced toxicity at lower concentrations (4 × MIC). The minimum concentration that produced the antibiofilm effect for AgNP-Aloe-1 and AgNP-Aloe-2 was 8 × MIC.

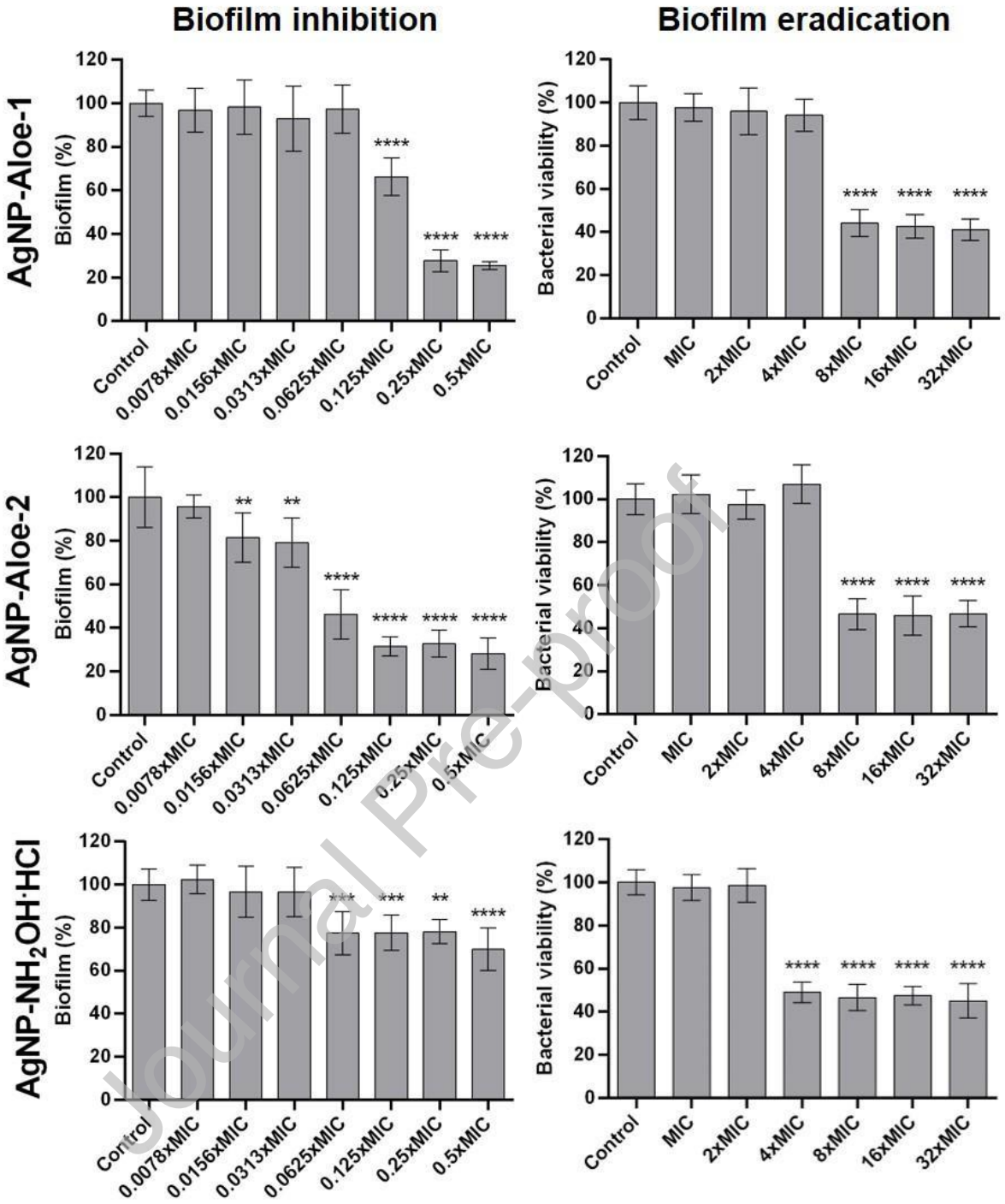

Figure 8. Antibiofilm activity of AgNP-Aloe-1, AgNP-Aloe-2, and AgNP-$NH_2OH{\cdot}HCl$. On one hand, the capability of AgNPs to inhibit the formation of *P. aeruginosa* biofilm was determined by CV staining (left) and, on the other hand, it was assessed their effect on pre-formed biofilm by means of MTT assay (right). The data are shown as mean ± SD (n = 6) and were analyzed using one-way ANOVA and the multiple comparisons tests of Dunnett. Each treatment was compared to the untreated control, ** $p < 0.01$, *** $p < 0.001$, **** $p < 0.0001$.

Although AgNPs have been proven to be effective antibacterial agents due to their size and shape, some articles suggest that the capping obtained during green synthesis plays a

relevant role in enhancing their antimicrobial activity [7]. It has been reported that *Aloe maculata* extract has antibacterial activity [18,19]. However, no antimicrobial activity was observed in this study when bacteria were incubated with the extract, even at the maximum concentration employed to synthetized the AgNPs. Nevertheless, the retention of phytocompounds, particularly on the surface of the AgNPs, may be related to the enhancement of the antibacterial efficacy. In particular, acemannan, which is one of the main components of the *Aloe maculata* extract [23] was indicated to augument the antibacterial effect of green-synthesized AgNPs [43]. Polyphenols are not responsible for the antibacterial properties in this case because they have not been detected in the AgNPs, and even though they were present in the extract, it did not show any antibacterial effect. The antioxidant activity determined from the AgNPs is not responsible for the antibacterial effect, since both the extract and the AgNPs showed similar antioxidant activities, and yet the extract alone did not exhibit antibacterial activity. A possible mechanism responsible for the improved antibacterial activity observed in this study, compared to AgNP-$NH_2OH{\cdot}HCl$, could be the capability of these nanoparticles to interact with the cell surface (Fig. 9). It has been reported that this kind of capping molecules can improve the binding ability of AgNPs to bacterial cells [44, 45]. Although the exact mechanism of action of AgNPs is still unknown, several studies indicate that AgNPs are able to physically interact with the cell surfaces of different bacteria [46]. However, the same capping could be involved in decreasing the efficacy of the AgNP-Aloe-1 and AgNP-Aloe-2 to eradicate a pre-formed biofilm, compared to AgNP-$NH_2OH{\cdot}HCl$. The extracellular matrix that surrounds the bacteria in the biofilm could interact with the phytocompounds, making it difficult for AgNPs to reach the bacteria surface. However, green-synthetized AgNPs presented better performance than AgNP-$NH_2OH{\cdot}HCl$ in preventing the biofilm formation. On the other hand, it is important to highlight that the concentrations with an antimicrobial effect were not toxic to skin cells.

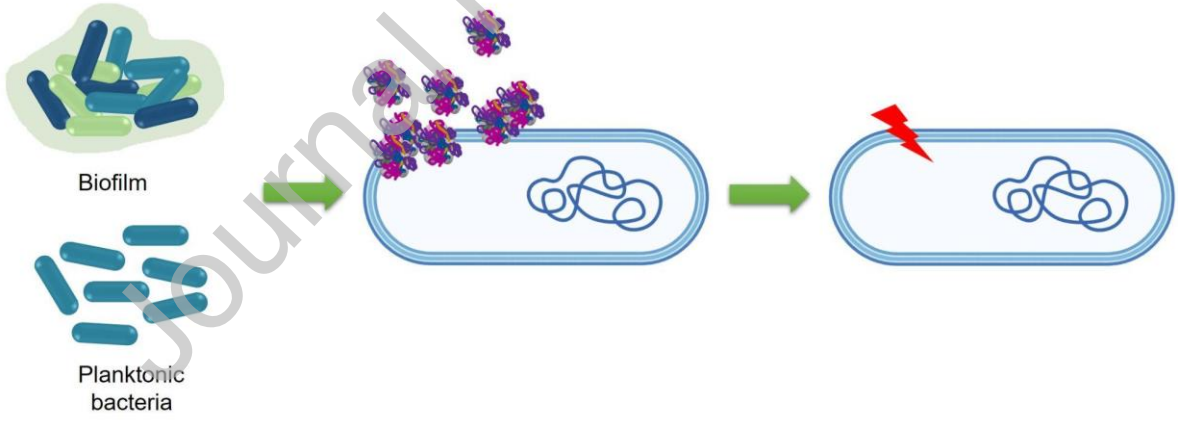

Figure 9. Representation of a possible mechanism of action for the novel AgNPs obtained by green synthesis using an *Alore maculata* aqueous extract. The AgNPs could interact with and disrupt the bacterial cell wall and membrane.

3.5 Human skin penetration of AgNPs

Figure 10 shows that all AgNPs could penetrate the SC and enter the VED. However, most of the signal for both green-synthesized AgNPs was detected in the SC —particularly in its shallow portion—, while AgNP-$NH_2OH{\cdot}HCl$ penetrated deeper with low recovery from the SC and most of the signal in the VED ($p < 0.0001$). This could be attributed to the plant-derived compounds that remain on the surface of the green-synthesized AgNPs, which could interact with the SC and slow down their penetration into deeper skin layers. These results suggest

that green-synthesized AgNPs could be useful in topical treatments as they exhibit an antibacterial effect and remain mainly retained in the SC.

A useful formulation of AgNPs should not significantly penetrate the highly vascularized dermis, where lymphatic drainage of the skin also occurs, to avoid potential systemic distribution with side effects. The concentrations used in the skin penetration assays (1600 µg/mL) were much higher than the MIC for *E. coli*, *S. aureus*, and *P. aeruginosa*. Therefore, the distribution in the dermis could be significantly lower whan using the therapeutic doses. Moreover, these assays were performed on intact skin samples, but in practical situations such as wound or burn treatments, the SC could be damaged, thus favoring the systemic distribution of the AgNPs. The low doses that showed antibacterial activity could minimize systemic side effects. Further *in vivo* testing should be performed to more precisely determine their therapeutic effect, local and systemic potential side effects, and distribution. Lastly, the activity against pre-formed biofilm and the preventive effect could make these AgNPs useful for diverse applications, from potential treatments to coating surgical elements, given the implications of biofilms in some skin afflictions such as atopic dermatitis or acne [47,48]. The presence of phytocompounds could also provide other healing effects that have to be determined in the future.

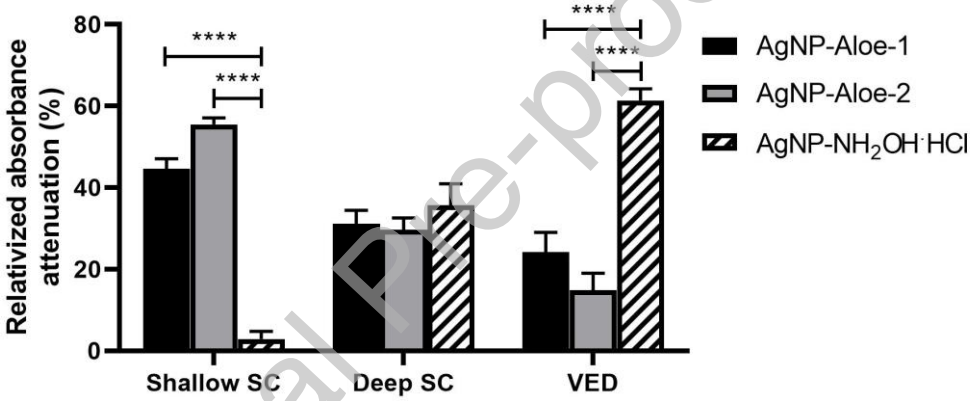

Figure 10. Relativized percentage of absorbance attenuation by forming Ag_2CrO_4 from a solution of K_2CrO_4 after incubation with extracts from skin tape stripping. In the presence of Ag^+, the absorbance of the solution at 375 nm decreases proportionally to the concentration of the ion due to the formation of the precipitate Ag_2CrO_4. Therefore, higher percentages of absorbance attenuation correspond to higher concentrations of Ag^+. Shallow SC corresponds to tapes 1-10, deep SC to tapes 11-20, and VED to viable epidermis and dermis. The data are shown as mean ± SEM (n = 3) and were analyzed using one-way ANOVA and the multiple comparisons tests of Dunnett. Green-synthetized AgNPs were compared to AgNP-$NH_2OH{\cdot}HCl$ (**** $p < 0.0001$).

4. Conclusions

In this study, the first AgNPs were synthesized using green synthesis from an *Aloe maculata* extract and were characterized. This study demonstrated the potential of this plant for green synthesis. These AgNPs showed antibacterial and antibiofilm activity at sub-toxic concentrations for skin cells. Moreover, in several of the conditions studied, they exhibited better performance against Gram-positive and Gram-negative bacteria compared to AgNPs obtained through traditional chemical synthesis. Although more exhaustive characterization of the conformation and mechanism of action of these AgNPs is necessary, the phytocompounds that remain anchored may be responsible for the differential effects

between green-synthesized AgNPs and those from traditional synthesis. Therefore, continuing the characterization studies of the extract is essential to achieve better reproducibility in obtaining these AgNPs from one harvest to another and to further understand their potential in treating skin diseases. It is also clear that these new AgNPs were not very stable in Milli-Q water over time, so conservation methods need to be improved. Additionally, the limited penetration of these novel AgNPs is another promising feature for topical application, as it reduces their systemic distribution. Therefore, these novel AgNPs have the potential to be used as antibacterial agents, especially for topical applications.

CONFLICT OF INTEREST DECLARATION:

We wish to confirm that there are no known conflicts of interest associated with this publication and there has been no significant financial support for this work that could have influenced its outcome.

In behalf of all the authors,

Dr. María Natalia Calienni
Researcher at CONICET (National Council of Science and Technology of Argentina)
National University of Hurlingham, Tte. Origone 151, (1688) V. Tesei, Buenos Aires, Argentina.
TE: +54911 15 66061124
natalia.calienni@unahur.edu.ar

Acknowledgments

Calienni, Montanari, Maffia, Alonso, and Lillo are members of CONICET Argentina. Corleto acknowledges a doctoral fellowship from CONICET and ANLAP and Sosa a doctoral fellowship from CONICET Argentina. This work was supported by grants from Universidad Nacional de Quilmes (PUNQ 1311/19), Universidad Nacional de Hurlingham (PIUNAHUR 2021), Universidad Nacional de Tucumán (D0639/1/3), and Consejo Nacional de Investigaciones Científicas y Técnicas (CONICET) (PIP 002).

References

[1] WHO, Antimicrobial resistance, (2021). https://www.who.int/news-room/fact-sheets/detail/antimicrobial-resistance.

[2] WHO, Lack of innovation set to undermine antibiotic performance and health gains, (2022). https://www.who.int/news/item/22-06-2022-22-06-2022-lack-of-innovation-set-to-undermine-antibiotic-performance-and-health-gains.

[3] T.C. Dakal, A. Kumar, R.S. Majumdar, V. Yadav, Mechanistic basis of antimicrobial actions of silver nanoparticles, Front. Microbiol. 7 (2016) 1831. https://doi.org/10.3389/fmicb.2016.01831.

[4] E. Urnukhsaikhan, B.-E. Bold, A. Gunbileg, N. Sukhbaatar, T. Mishig-Ochir, Antibacterial activity and characteristics of silver nanoparticles biosynthesized from Carduus crispus, Sci. Rep. 11 (2021) 1–12. https://doi.org/10.1038/s41598-021-00520-2.

[5] M. Rafique, I. Sadaf, M.S. Rafique, M.B. Tahir, A review on green synthesis of silver nanoparticles and their applications, Artif. Cells, Nanomedicine, Biotechnol. 45 (2017) 1272–1291. https://doi.org/10.1080/21691401.2016.1241792.
[6] S. Ahmed, M. Ahmad, B.L. Swami, S. Ikram, A review on plants extract mediated synthesis of silver nanoparticles for antimicrobial applications: a green expertise, J. Adv. Res. 7 (2016) 17–28. https://doi.org/10.1016/j.jare.2015.02.007.
[7] Rai, M.; Ingle, A.P.; Trzcińska-Wencel, J.; Wypij, M.; Bonde, S.; Yadav, A.; Kratošová, G.; Golińska, P. Biogenic Silver Nanoparticles: What We Know and What Do We Need to Know? Nanomaterials 2021, 11, 2901. https://doi.org/10.3390/nano11112901
[8] A. Rastogi, P. Singh, F.A. Haraz, A. Barhoum, Biological synthesis of nanoparticles: An environmentally benign approach, in: Fundam. Nanoparticles, Elsevier, 2018: pp. 571–604. https://doi.org/10.1016/B978-0-323-51255-8.00023-9.
[9] A.A. Yaqoob, K. Umar, M.N.M. Ibrahim, Silver nanoparticles: various methods of synthesis, size affecting factors and their potential applications–a review, Appl. Nanosci. 10 (2020) 1369–1378. https://doi.org/10.1007/s13204-020-01318-w.
[10] S. Dawadi, S. Katuwal, A. Gupta, U. Lamichhane, R. Thapa, S. Jaisi, G. Lamichhane, D.P. Bhattarai, N. Parajuli, Current research on silver nanoparticles: Synthesis, characterization, and applications, J. Nanomater. 2021 (2021). https://doi.org/10.1155/2021/6687290.
[11] T.R. Anju, S. Parvathy, M.V. Veettil, J. Rosemary, T.H. Ansalna, M.M. Shahzabanu, S. Devika, Green synthesis of silver nanoparticles from Aloe vera leaf extract and its antimicrobial activity, Mater. Today Proc. 43 (2021) 3956–3960. https://doi.org/10.1016/j.matpr.2021.02.665
[12] H. Arshad, M. Saleem, U. Pasha, S. Sadaf, Synthesis of Aloe vera-conjugated silver nanoparticles for use against multidrug-resistant microorganisms, Electron. J. Biotechnol. 55 (2022) 55–64. https://doi.org/10.1016/j.ejbt.2021.11.003.
[13] Grace, O. M., Simmonds, M. S. J., Smith, G. F., & van Wyk, A. E. (2008). Therapeutic uses of Aloe L. (Asphodelaceae) in southern Africa. Journal of Ethnopharmacology, 119(3), 604–614. doi:10.1016/j.jep.2008.07.002
[14] El Sayed, A. M., Ezzat, S. M., El Naggar, M. M., & El Hawary, S. S. (2016). In vivo diabetic wound healing effect and HPLC-DAD-ESI-MS/MS profiling of the methanol extracts of eight Aloe species. Revista Brasileira de Farmacognosia, 26, 352-362.
[15] K. Adlakha, B. Koul, A. Kumar, Value-added products of Aloe species: Panacea to several maladies, South African J. Bot. (2021). https://doi.org/10.1016/j.sajb.2020.12.025.
[16] Jasso de Rodriguez, D. J., Angulo-Sanchez, J. L., da Silva, J. A. T., & Aguilar-Gonzalez, C. N. (2006). Review of Aloe species' medicinal properties and bioactive compounds. Floriculture, ornamental and plant biotechnology, 460-471.
[17] Yoo, E. A., Kim, S. D., Lee, W. M., Park, H. J., Kim, S. K., Cho, J. Y., ... & Rhee, M. H. (2008). Evaluation of antioxidant, antinociceptive, and anti- inflammatory activities of ethanol extracts from Aloe saponaria Haw. Phytotherapy Research: An International Journal Devoted to Pharmacological and Toxicological Evaluation of Natural Product Derivatives, 22(10), 1389-1395.
[18] Cock, I. E., & Van Vuuren, S. F. (2020). The traditional use of southern African medicinal plants for the treatment of bacterial respiratory diseases: A review of the ethnobotany and scientific evaluations. Journal of ethnopharmacology, 263, 113204.
[19] Sonam, S. K., & Tiwari, A. (2015). Antibacterial efficacy of aloe species on pathogenic bacteria. Int J Sci Technol Manag, 4(1), 143-151.
[20] Sedaghathoor, S., Kojeidi, M. I., & Poormassalegoo, A. (2017). Study on the effect of brassinolide and salicylic acid on vegetative and physiological traits of Aloe maculata All. in different substrates in a pot experiment. Journal of applied research on medicinal and aromatic plants, 6, 111-118.
[21] Kim, H., Kim, B. W., Yoo, D., Moon, J., Kwon, I., Lee, Y., & Seo, J. (2023). In vitro evaluation of Aloe saponaria as a potential feed additive to modulate ruminal fermentation and microbial diversity. Journal of Applied Animal Research, 51(1), 115-

122.
[22] Silva, M. A., Trevisan, G., Klafke, J. Z., Rossato, M. F., Walker, C. I. B., Oliveira, S. M., & Ferreira, J. (2013). Antinociceptive and anti-inflammatory effects of Aloe saponaria Haw on thermal injury in rats. Journal of ethnopharmacology, 146(1), 393-401.
[23] M. Beverina, S. Sanchez-Cortes, F.I. Schabes, J. Zapata, M.L.A. Cassará, M.E. Tuttolomondo, Spectroscopic characterization (Raman and infrared) of Aloe maculata from the north Argentina region, Vib. Spectrosc. 122 (2022) 103423. https://doi.org/j.vibspec.2022.103423.
[24] N. Leopold, B. Lendl, A new method for fast preparation of highly surface-enhanced Raman scattering (SERS) active silver colloids at room temperature by reduction of silver nitrate with hydroxylamine hydrochloride, J. Phys. Chem. B. 107 (2003) 5723–5727. https://doi.org/10.1021/jp027460u.
[25] E. Lopez-Tobar, B. Hernández, M. Ghomi, S. Sanchez-Cortes, Stability of the disulfide bond in cystine adsorbed on silver and gold nanoparticles as evidenced by SERS data, J. Phys. Chem. C. 117 (2013) 1531–1537. https://doi.org/10.1021/jp3112606.
[26] Montanari J, Vera M, Mensi E, Morilla M, Romero E. Nanoberries for topical delivery of antioxidants. J Cosmet Sci. 2013 Nov-Dec;64(6) 469-481. PMID: 24397884..
[27] M.N. Calienni, D. Maza Vega, C.F. Temprana, M.C. Izquierdo, D.E. Ybarra, E. Bernabeu, M. Moretton, F.C. Alvira, D. Chiappetta, S. del V. Alonso, M.J. Prieto, J. Montanari, The Topical Nanodelivery of Vismodegib Enhances Its Skin Penetration and Performance In Vitro While Reducing Its Toxicity In Vivo, Pharmaceutics. 13 (2021) 186. https://doi.org/10.3390/pharmaceutics13020186.
[28] M. Martinez, S. Gonçalves, M.R. Felício, P. Maturana, N.C. Santos, L. Semorile, A. Hollmann, P.C. Maffía, Synergistic and antibiofilm activity of the antimicrobial peptide P5 against carbapenem-resistant Pseudomonas aeruginosa, Biochim. Biophys. Acta (BBA)-Biomembranes. 1861 (2019) 1329–1337. https://doi.org/10.1016/j.bbamem.2019.05.008
[29] Methods for Dilution Antimicrobial Susceptibility Tests for Bacteria That Grow Aerobically; Approved Standard—Ninth Edition. January 2012, M07-A9 Vol. 32 No. 2, Replaces M07-A8 Vol. 29 No. 2
[30] M. Martínez, A. Polizzotto, N. Flores, L. Semorile, P.C. Maffía, Antibacterial, anti-biofilm and in vivo activities of the antimicrobial peptides P5 and P6. 2, Microb. Pathog. 139 (2020) 103886. https://doi.org/10.1016/j.micpath.2019.103886.
[31] U. Schaefer, H. Loth, An ex-vivo model for the study of drug penetration into human skin, Pharm. Res. 13 (1996) b24.
[32] M.N. Calienni, C. Febres-Molina, R.E. Llovera, C. Zevallos-Delgado, M.E. Tuttolomondo, D. Paolino, M. Fresta, H.L. Barazorda-Ccahuana, B. Gómez, S. del V. Alonso, J. Montanari, Nanoformulation for potential topical delivery of Vismodegib in skin cancer treatment, Int. J. Pharm. 565 (2019) 108–122. https://doi.org/10.1016/j.ijpharm.2019.05.002.
[33] H. Ashraf, T. Anjum, S. Riaz, S. Naseem, Microwave-assisted green synthesis and characterization of silver nanoparticles using Melia azedarach for the management of Fusarium wilt in tomato, Front. Microbiol. 11 (2020) 238. https://doi.org/10.3389/fmicb.2020.00238.
[34] P. Tippayawat, N. Phromviyo, P. Boueroy, A. Chompoosor, Green synthesis of silver nanoparticles in aloe vera plant extract prepared by a hydrothermal method and their synergistic antibacterial activity, PeerJ. 4 (2016) e2589. https://doi.org/10.7717/peerj.2589.
[35] M. Vanaja, K. Paulkumar, M. Baburaja, S. Rajeshkumar, G. Gnanajobitha, C. Malarkodi, M. Sivakavinesan, G. Annadurai, Degradation of methylene blue using biologically synthesized silver nanoparticles, Bioinorg. Chem. Appl. 2014 (2014). https://doi.org/10.1155/2014/742346.
[36] Moosa, A. A., Ridha, A. M., & Al-Kaser, M. (2015). Process parameters for

green synthesis of silver nanoparticles using leaves extract of Aloe vera plant. Int J Multi Curr Res, 3, 966-975. (es en el que se basaron para la sint de las AgNPs)
[37] Patil Shriniwas, P.; Kumbhar Subhash, T. Antioxidant, antibacterial and cytotoxic potential of silver nanoparticles synthesized using terpenes rich extract of Lantana camara L. leaves. Biochem. Biophys. Rep. 2017, 10, 76–81.
[38] Hęś, M., Dziedzic, K., Górecka, D., Jędrusek-Golińska, A., & Gujska, E. (2019). Aloe vera (L.) Webb.: natural sources of antioxidants–a review. Plant Foods for Human Nutrition, 74, 255-265
[39] Kang, J. R., Kim, G. M., & Shin, J. H. (2022). Anti-inflammatory activities of polysaccharides isolated from Aloe saponaria Haw grown in Namhae. Korean Journal of Food Preservation, 29(7), 1189-1200.
[40] G. Repetto, A. Del Peso, J.L. Zurita, Neutral red uptake assay for the estimation of cell viability/cytotoxicity, Nat. Protoc. 3 (2008) 1125. https://doi.org/10.1038/nprot.2008.75.
[41] T. Jaswal, J. Gupta, A review on the toxicity of silver nanoparticles on human health, Mater. Today Proc. (2021). https://doi.org/10.1016/j.matpr.2021.04.266.
[42] S. Pugazhendhi, P. Sathya, P.K. Palanisamy, R. Gopalakrishnan, Synthesis of silver nanoparticles through green approach using Dioscorea alata and their characterization on antibacterial activities and optical limiting behavior, J. Photochem. Photobiol. B Biol. 159 (2016) 155–160. https://doi.org/10.1016/j.jphotobiol.2016.03.043
[43] Anju, T. R., Parvathy, S., Veettil, M. V., Rosemary, J., Ansalna, T. H., Shahzabanu, M. M., & Devika, S. (2021). Green synthesis of silver nanoparticles from Aloe vera leaf extract and its antimicrobial activity. Materials Today: Proceedings, 43, 3956-3960.
[44] El-Rafie, M.H.; El-Naggar, M.E.; Ramadan, M.A.; Fouda, M.M.G.; Al-Dey, S.S.; Hebeish, A. Environmental synthesis of silver nanoparticles using hydroxypropyl starch and their characterization. Carbohydr. Polym. 2011, 86, 630–635. [CrossRef]
[45] Roy, A.; Bulut, O.; Some, S.; Kumar Mandal, A.; Yilmaz, M.D. Green synthesis of silver nanoparticles: Biomolecule-nanoparticle organizations targeting antimicrobial activity. RSC Adv. 2019, 9, 2673–2702.
[46] Mikhailova, E.O. Silver Nanoparticles: Mechanism of Action and Probable Bio-Application. J. Funct. Biomater. 2020, 11, 84
[47] M. Brandwein, D. Steinberg, S. Meshner, Microbial biofilms and the human skin microbiome, NPJ Biofilms Microbiomes. 2 (2016) 1–6. https://doi.org/10.1038/s41522-016-0004-z.
[48] K.V. Vaishnavi, L. Safar, K. Devi, Biofilm in dermatology, J. Ski. Sex. Transm. Dis. 1 (2019) 3–7. https://doi.org/10.25259/JSSTD_14_2019.